Intensity effects in ultracold photoassociation line shapes

A. Simoni,* P. S. Julienne, E. Tiesinga, and C. J. Williams
Atomic Physics Division, National Institute of Standards and Technology, Gaithersburg, Maryland 20899-8423
(Received 25 July 2002; published 13 December 2002)

We derive ultracold atom-atom photoassociation line shapes valid for intense light fields and investigate laser power effects in sodium and rubidium photoassociation to the purely long-range 0_g^- symmetry state. We consider intensities up to a few hundreds W/cm^2, a strongly saturating intensity for typical transitions of experimental interest. For these intensities the 0_g^- rotational spectrum is still well resolved; however, it is essential to couple the photoassociation resonance to both *s*- and *d*-wave ground-state channels. A low-energy *d*-wave shape resonance can have a profound effect on the line shape. Understanding the line shape is essential for precision spectroscopic analysis and could improve the extraction of ground-state scattering properties such as scattering lengths.

DOI: 10.1103/PhysRevA.66.063406 PACS number(s): 32.80.Pj, 34.50.Rk, 33.70.Jg

I. INTRODUCTION

Photoassociative spectroscopy of ultracold gases [1] has provided important information about ground-state collisions between alkali-metal atoms [2–6]. The success of photoassociation (PA) spectroscopy in determining ground-state collision parameters relies on the relation between observed shapes and relative strengths of different rovibrational lines and the structure of the scattering wave function [7]. Although many groups are aware [8,9] of intensity effects on PA line shapes, most previous analyses of PA line shapes has been carried out in a low intensity and unsaturated regime since higher intensity effects have not been fully understood. Intensity effects have been discussed with respect to light shifts [10–12] and scattering length modification [13]. In the low intensity limit perturbative theories are in excellent agreement with the experiments, and the lines are described by a Lorentzian curve [14] arising from a single excitation of the colliding atomic fragments to the quasi-molecular bound level and the subsequent decay or detection of the intermediate state. Photoassociation beyond the linear response regime is, however, nonperturbative and can be described as a sum of virtual excitations and deexcitations involving all the states coupled by the radiation field [15]. As a consequence of the interaction, PA spectra in this regime show subtle laser-induced level shifts and broadening.

A main purpose of this paper is to investigate the dependence of level shifts and broadening of PA lines on the collision energy and to explore the consequences of this dependence when a thermal gas is photoassociated. In addition, the effects of coupling of different partial waves through the excited state are especially profound when there are ground-state shape resonances (Fig. 1 shows a schematic representation of the process). There is a nontrivial interplay between shifts and broadening that can result in unexpected thermal line shapes. In particular, the energy dependence of level shifts and broadening can result in shifts without broadening and broadening without shifts.

The paper is organized as follows. In Sec. II we describe the model and outline the analytic derivation of the line shape in a near-resonant approximation. We illustrate the model by a choice of atomic states and field polarization that set up a two- or three-channels problem. In Sec. III numerical results are provided for PA of a ^{23}Na cold gas, showing the strong effect of a *d*-wave shape resonance even though its position is $E_r \approx 10 k_B T$ above threshold, where k_B is the Boltzmann constant and T is the temperature of the gas under consideration. Section IV focuses on ^{87}Rb PA, describing the effect on the line shapes of a low-energy $E_r \approx k_B T$ *d*-wave

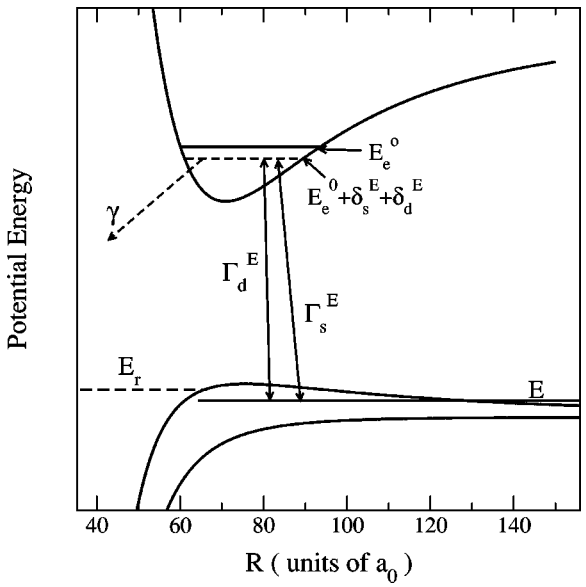

FIG. 1. Sketch of a high-intensity photoassociation process for Na (vertical axis is not to scale). Two atoms colliding with angular momentum l ($l=0,2$ in this example) at collision energy E approach along the ground-state potential and are excited with rate Γ_l^E to an excited level E_e^0. Excited molecules can decay with rate γ by spontaneous emission (dashed arrow) or be recoupled to the ground state with an l generally different from the incoming one (solid arrows). The total shift $\delta_s^E+\delta_d^E$ of the excited level depends on all the ground-state continua coupled by the field. The long-dashed line represents a *d*-wave shape resonance at energy E_r in the ground-state potential.

*Also at INFM and LENS, Università di Firenze, Largo E. Fermi 2, I-50125 Firenze, Italy.

shape resonance. From these complicated saturated line shapes we show how to determine the resonance positions. This is followed in Sec. V by some concluding remarks.

II. MODEL

We model one color photoassociation of two ground-state alkali-metal atoms to the first excited molecular state. The laser mode will be labeled by the field wave vector $\mathbf{k}$ and polarization $\boldsymbol{\epsilon}$. The theory assumes a negligible strength for two-photon transitions to higher molecular states. The PA process can be cast as a scattering close-coupling problem in a basis of light-dressed molecular states [16,17] defined as $|lm\alpha N_{\mathbf{k}\boldsymbol{\epsilon}}\rangle$. The quantum number α specifies the internal state of a pair of noninteracting atoms, l is the relative orbital angular momentum, m is the projection of l on a space quantization axis, and $N_{\mathbf{k}\boldsymbol{\epsilon}}$ is the photon number in the laser mode. As the atoms approach each other the various ground- and excited-state channels $|lm\alpha N_{\mathbf{k}\boldsymbol{\epsilon}}\rangle$ are coupled both directly by the molecular interatomic potentials and by the indirect atom-field interaction. There are in general N_g ground-state channels and N_e excited-state channels which can be selectively coupled through the radiation field. In order to simplify notation, we henceforth drop the symbols m and $N_{\mathbf{k}}$ unless needed for clarity.

In the dressed-state representation the multichannel Hamiltonian of the system can be written as $H=K+V$ where $K=-\mathbf{1}(\hbar^2/2\mu)d^2/dr^2$ is the relative radial kinetic energy, μ the reduced mass, and

$$V=\begin{pmatrix} V_{gg} & V_{ge} \\ V_{eg} & V_{ee}-\hbar\omega\mathbf{1}_{ee}-\dfrac{i}{2}\gamma \end{pmatrix}$$

is the total potential energy including spontaneous decay. The matrices $\mathbf{1}$ and $\mathbf{1}_{ee}$ are unit matrices of dimension $(N_g+N_e)\times(N_g+N_e)$ and $(N_e\times N_e)$, respectively. The ground-state potential V_{gg} of dimension $(N_g\times N_g)$ includes the electrostatic interaction between two ground-state atoms, the atomic hyperfine energy and the rotational Hamiltonian of the atoms about the center of mass. At large internuclear separation V_{gg} tends to a diagonal matrix V_{gg}^{∞} whose elements are given by the atomic hyperfine energies. At collision energy E, N_0 ground-state channels will be open. In general N_0 will be smaller than N_g. The excited-state potential V_{ee} of dimension $(N_e\times N_e)$ contains the same terms as the ground-state potential plus the spin-orbit interaction. Asymptotically V_{ee} tends to a diagonal matrix V_{ee}^{∞} whose elements are given by the spin-orbit plus hyperfine energy.

The matrix $\hbar\omega\mathbf{1}_{ee}$ represents the reduction in the energy of the laser field due to the absorption of a photon. In the PA experiments that we consider the photon frequency is such that $E\ll(V_{ee}^{\infty})_{ii}-\hbar\omega$, i.e., all excited states are closed asymptotically. The atoms-field coupling, the $(N_g\times N_e)$ matrix V_{ge}, is given by

$$V_{ge}(r)=-d(r)\sqrt{\frac{2\pi I}{c}},$$

where I is the laser intensity, c is the speed of light, and d is the molecular electric-dipole moment matrix.

The imaginary term $i\gamma$ in the excited state accounts for spontaneous emission and any other *irreversible* flux losses from the excited state not contained within the model [18,19]. Use of this imaginary term is limited to conditions where reexcitation of decayed population can be neglected. At the laser cooling temperatures considered in this paper, Doppler effects due to the molecule center-of-mass motion and the recoil energy of the absorbed photon can be neglected. In order to cast the problem as a scattering problem it is necessary to impose boundary conditions using asymptotic channel states that are diagonal in the atomic *plus* radiative Hamiltonian [20]. Some effects of a proper definition of the boundary conditions, or dressing effects, have been investigated in Ref. [21] for a two-state model. In this paper we assume that the atoms do not interact with the light field at large internuclear distance and let the radiative coupling V_{ge} asymptotically vanish. The rationale for this choice is that the numerical calculations show that dressing effects can be neglected at typical laser cooling temperatures for intensities below a few W/cm^2. In addition, even for higher intensities, since the results only depend on excitation near the Condon point, asymptotic dressing effects do not qualitatively change our conclusions about the PA line shape.

With this proviso, in the next section we derive a formal analytic expression which explicitly shows the dependence of transition T-matrix elements on the laser frequency and intensity. Use of the analytic form of the transition matrix will allow a much simpler investigation of saturation phenomena as compared to a full close-coupling calculation.

A. Analytic theory

The transition T matrix is derived by dividing the potential V into a molecular, V_0, and a radiative, V_r, component:

$$V\equiv V_0+V_r,$$

$$V_0=\begin{pmatrix} V_{gg} & 0 \\ 0 & V_{ee}-\hbar\omega\mathbf{1}_{ee} \end{pmatrix},\quad V_r=\begin{pmatrix} 0 & V_{ge} \\ V_{eg} & -\dfrac{i}{2}\boldsymbol{\gamma} \end{pmatrix}$$

and by defining projection operators P and Q onto subspaces spanned by the ground and excited channels, respectively. Then we can use the two-potentials scattering formula [22]

$$\langle El'\beta|T|El\alpha\rangle=\langle El'\beta|T_0|El\alpha\rangle+\langle\Phi_{l'\beta}^{E(-)}|V_r|\Psi_{l\alpha}^{E(+)}\rangle \tag{1}$$

to formally represent the transition T-matrix element from channel $\{l\alpha\}$ to channel $\{l'\beta\}$ at total energy E as a sum of the transition matrix T_0 for scattering from the molecular potential plus a matrix element of the radiative coupling V_r. In Eq. (1) $|\Psi_{l\alpha}^{E(+)}\rangle$ is the scattering state for the potential V and particles incoming in channel $l\alpha$. The state $|\Phi_{l'\beta}^{E(-)}\rangle$ is the scattering state for the potential V_0 and particles outgoing in channel $l'\beta$. The last term on the right-hand side of Eq. (1) can be rewritten as

$$\langle \Phi^{E(-)}_{l'\beta}|V_r|\Psi^{E(+)}_{l\alpha}\rangle = \langle \Phi^{E(-)}_{l'\beta}|V_{ge}G^{(+)}_{ee}(E)V_{eg}|\Phi^{E(+)}_{l\alpha}\rangle,$$

involving only scattering wave functions for the potential V_0 and an effective propagator for the excited state $G^{(+)}_{ee}(E)$ given by [23]

$$G^{(+)}_{ee}(E) = \frac{Q}{Q(E-H^0-V_rPG^{(+)}_0PV_r)Q+\frac{i}{2}\boldsymbol{\gamma}}, \qquad (2)$$

where $H^0=K+V_0$ and $G_0(z)=(z-H^0)^{-1}$ is the field-free propagator. The superscript $(+)$ of the propagators denote outgoing boundary conditions.

We are interested in a situation where the energies E^0_{ei} of only a small number of bound states $\{\Phi^0_{ei}\}$ of the potential V_{ee} are nearly resonant with the laser. Consequently, $G^{(+)}_{ee}(E)$ is a finite-size matrix. Latin letters will henceforth be used to label these excited states. The terms $Q(E-H^0)Q$ and γ of the denominator are diagonal in the basis $\{\Phi^0_{ei}\}$ with elements equal to $(E+\hbar\omega-E^0_{ei})$ and γ_i, respectively. The complex matrix $\langle\Phi^0_{ej}|V_{eg}PG^{(+)}_0(E)PV_{ge}|\Phi^0_{ei}\rangle = \delta^E_{ij}+(i/2)\Gamma^E_{ij}$, where the symmetric matrix

$$\Gamma^E_{ij} = \sum_{\alpha=1}^{N_0}\sum_l \Gamma^E_{ijl\alpha},$$
$$\Gamma^E_{ijl\alpha} \equiv 2\pi\langle\Phi^0_{ej}|V_{eg}|\Phi^{E(+)}_{l\alpha}\rangle\langle\Phi^{E(+)}_{l\alpha}|V_{ge}|\Phi^0_{ei}\rangle \qquad (3)$$

is the light-induced broadening, and the symmetric matrix

$$\delta^E_{ij} = \sum_{\alpha=1}^{N_g}\sum_l \delta^E_{ijl\alpha} + \sum_{ln}\delta^E_{ijln},$$

$$\delta^E_{ijl\alpha} = \frac{1}{2\pi}\mathcal{P}\int_{E^\infty_\alpha}^{\infty}\frac{\Gamma^{E'}_{ijl\alpha}}{E-E'}dE', \qquad (4)$$

$$\delta^E_{ijln} = \frac{\langle\Phi^0_{ej}|V_{eg}|\Phi^0_{gln}\rangle\langle\Phi^0_{gln}|V_{ge}|\Phi^0_{ei}\rangle}{E-E^0_{gln}}$$

is the light induced level shift. Here $\mathcal{P}$ denotes the Cauchy principal-value integral and $\{ln\}$ label the discrete eigenvalues E^0_{gln} and eigenvectors $|\Phi^0_{gln}\rangle$ of the ground-state potential V_{gg}. The matrices Γ and δ are independent of laser frequency and are linear in the intensity. Only open channels contribute to the broadening matrix Γ, while both open and closed channels contribute to the shift matrix δ. Off-diagonal elements of $\delta+(i/2)\Gamma$ represent indirect couplings between the excited states through the ground states.

The contribution of the principal-value integral to the diagonal elements of the shift matrix is negative (redshift) in the zero-energy limit. Loosely speaking this is because for $E\to 0$ there is always ''more continuum'' above than below the total energy E. However we will show in Sec. III that this is not always true at finite temperature. Bound-bound contributions are always positive (blueshift) and for cold collisions can become relevant when a bound state in the ground-state potential is close to threshold and has a significant overlap with the excited state. An example of this situation will be given in Sec. III.

An alternative form for the level shift involving the regular and the irregular solutions of the scattering equations is provided in Ref. [10]. The level-shift expression of Ref. [10] is more convenient for numerical calculations as it involves scattering wave functions evaluated at a single collision energy; however, in order to show the individual continuum-bound and bound-bound contributions to the shift, we use Eq. (4) in this paper.

Summarizing, the T matrix is

$$\langle El'\beta|T|El\alpha\rangle = \langle El'\beta|T_0|El\alpha\rangle + \sum_{ij}\langle\Phi^{E(-)}_{l'\beta}|V_{ge}|\Phi^0_{ei}\rangle \times [G^{(+)}_{ee}(E)]_{ij}\langle\Phi^0_{ej}|V_{eg}|\Phi^{E(+)}_{l\alpha}\rangle, \qquad (5)$$

where

$$[G^{(+)}_{ee}]_{ij} = \left[(E+\hbar\omega)\mathbf{1}_{ee}-E^0_e-\delta+\frac{i}{2}(\gamma+\Gamma)\right]^{-1}_{ij}.$$

This expression is nonperturbative and therefore virtual excitation and deexcitation processes are included to all orders. In the absence of spontaneous emission the scattering operator $S=(\mathbf{1}-2\pi iT)$ is unitary.

When $\gamma\neq 0$ the partial event rate constant $\mathcal{L}_{\alpha lm}$ for loss of atoms from the excited states due to atoms colliding with internal state α and orbital angular momentum l and projection m is proportional to the loss of unitarity of the S matrix:

$$\mathcal{L}_{\alpha lm} = \frac{\pi v_\alpha}{k^2_\alpha}\left(1-\sum_{\beta l'm'}|S_{\beta l'm',\alpha lm}|^2\right) \equiv \frac{\pi v_\alpha}{k^2_\alpha}p_{\alpha lm}, \qquad (6)$$

where v_α is the asymptotic relative velocity in channel α and $p_{\alpha lm}$ is the probability per collision event of atom loss from the trap due to irreversible decay of the excited level. Here we assume that all decay processes that contribute to γ lead to loss of trapped atoms. If this were not the case, one would need to replace γ in the numerator of Eqs. (9) and following by $f\gamma$, where f is the fraction of irreversible decay that does lead to loss of trapped atoms. In this way, one could account for the fact that not all spontaneous decay necessarily leads to loss of atoms, since some may be slow enough to remain trapped.

Thermal averaging at temperature T requires

$$\mathcal{R}_{\alpha lm}(\omega,I,T) \equiv \langle\mathcal{L}_{\alpha lm}\rangle = \left\langle\frac{\pi v_\alpha}{k^2_\alpha}p_{\alpha lm}\right\rangle. \qquad (7)$$

Finally, the total event rate constant from state α, which gives the PA line shape in an experiment, is proportional to $\Sigma_{lm}\mathcal{R}_{\alpha,lm}$.

B. Line shapes

In order to use the above formalism, we need to define the channel indexes α for alkali-metal atoms. Assuming that the

atoms are trapped in a weak magnetic and/or optical external field, the hyperfine angular momentum of each atom $\mathbf{f}_a = \mathbf{s}_a + \mathbf{i}_a$, where $\mathbf{s}_a$ and $\mathbf{i}_a$ are the respective electron and nuclear angular momenta, is conserved to a good approximation. Thus, the ground-state index is $\alpha \equiv \{f_a f_b m_{fa} m_{fb}\}$. We will illustrate the theory for both Na and Rb with a simple yet experimentally realizable case in which the atoms are prepared in the ''stretched state,'' where $m_{fa} = f_a = i_a + 1/2$. For this state the ground-state collision is described by a single adiabatic Born-Oppenheimer potential of $^3\Sigma_u^+$ molecular symmetry.

For the excited state, we consider rotational levels of the purely long-range Hund's case (c) 0_g^- state discussed in detail in [24]. The molecular rotational angular momentum $\mathbf{J}'$ and the total nuclear spin $\mathbf{I}'$ are approximately good quantum numbers for the lower vibrational levels. For Na we treat the $\{J'=2\}$ feature, the strongest one for the PA spectrum of the purely long-range 0_g^- state. This feature can only have contributions from ground state *s*-, *d*- and *g*-wave collisions [24]. Choosing σ^- polarized light propagating along the quantization direction of the external field, and limiting our analysis to $m=0$ collisions, dipole selection rules reduce the problem to the ground-state channels, which we here call Hund's case (m):

$$|l\rangle \equiv |\{f_a=2,\, f_b=2,\, m_{fa}=2,\, m_{fb}=2\},\, l, m=0\rangle \qquad (8)$$

for $l=0,2,4$ (s,d,g) and to the single excited molecular state

$$|1'\rangle = |0_g^-, J'=2,\, M_J'=0,\, I'=3,\, M_I'=3\rangle.$$

The molecular dipole moment is evaluated by firstly writing the 0_g^- state as an *r*-dependent linear combination of Hund's case (a) wave functions $|0_g^-\rangle = a(r)|^3\Sigma_g\rangle + b(r)|^3\Pi_g\rangle$ and secondly using a case $(m)\rightarrow(a)$ frame transformation in the ground state. It is then possible to express the required case $(a)\leftrightarrow(m)$ molecular dipole in terms of case $(a)\leftrightarrow(a)$ molecular dipoles.

Equation (6) for the event rate constant for $m=0$ collisions has the Lorentzian form:

$$\mathcal{L} = \mathcal{L}_s + \mathcal{L}_d + \mathcal{L}_g,$$
$$\mathcal{L}_l = \frac{\pi v}{k^2} \frac{\gamma \Gamma_l^E}{\left(E - \Delta - \sum_l \delta_l^E\right)^2 + \frac{1}{4}\left(\gamma + \sum_l \Gamma_l^E\right)^2}, \qquad (9)$$

where $\Delta = E_{e1'}^0 - \hbar\omega$ is the detuning, and $\Gamma_l^E = \Gamma_{1'1'l}$ using Eq. (8) for the ground state in Eq. (3), and the summation is over $l=0,2,4$. The partial contributions to the shift, δ_l^E, are defined similarly for $l=0,2,4$. For notational convenience the vibrational quantum number v of the excited state is not explicitly written. A notable feature of the line shape above is that the total shift and width in the denominator are given by a sum over individual partial-wave contributions. The denominator is the same for all incoming l's. For a sufficiently cold gas, it may be possible to neglect Γ_l $(l>0)$ with respect to Γ_s because of the Wigner's threshold law $\Gamma_l \sim E^{l+(1/2)}$ [20,25]. However, this is typically not possible for laser-cooled gases.

In contrast to the width Γ_l, the level shift is independent of energy in the Wigner threshold regime, and the *s*-wave contribution at low energy need not be the largest. The latter is because the principal part integral in Eq. (4) is slowly converging with respect to integration over E for all l values and has significant contributions from collision energies well above the *l*-wave $(l>0)$ centrifugal barrier, where $\Gamma_l (l>0)$ is comparable to Γ_s. Indeed, in some instances the *d* wave can give the dominant contribution to the shift even for a Bose-condensed gas [12].

The PA line shape for an actual experiment is a sum of contributions from each m, which excites a different M_J' sublevel of the $\{J'=2\}$ state. Since the shift and width depend in general on the sublevel, the incoherent sum over all levels will result in additional inhomogeneous broadening. Here we focus only on the $|1'\rangle$ sublevel and ground state $m=0$ in order to demonstrate the subtle effects of intensity and of a shape resonance on the line profile. The δ_{lm}^E and Γ_{lm}^E of the other sublevels are related to the ones calculated here by simple yet elegant angular momentum algebra through the Wigner-Eckart theorem, and could be worked out for any particular experimental situation.

In addition to investigating a $\{J'=2\}$ line shape, we will also discuss a $\{J'=4\}$ case, for which there is no *s*-wave contribution. In this case the line shape of Eq. (9) is also valid for the $\{J'=4\}$ state by replacing l with $l+2$. A similar line shape can be derived for a $\{J'=0\}$ state.

For ^{87}Rb PA we are primarily interested in line shapes arising from *d*-wave collisions of stretched state atoms. In order to avoid complications associated with a *g*-wave shape resonance [9], we choose to study a purely long-range 0_g^- $J'=0$ excited level. By choosing σ_z polarized light propagating in the trapping field direction, *s*-wave collisions are excluded, and the only states coupled by the field are the *d*-wave ground state

$$|1\rangle = |\{f_a=2,\, f_b=2,\, m_{fa}=2,\, m_{fb}=2\},\, l=2,\, m=-1\rangle$$

and the excited molecular state

$$|1'\rangle = |0_g^-, J'=0,\, I'=3,\, M_I'=3\rangle.$$

For these conditions, the total event rate,

$$\mathcal{L} = \frac{\pi v}{k^2} \frac{\gamma \Gamma_d^E}{(E - \Delta - \delta_d^E)^2 + \frac{1}{4}(\gamma + \Gamma_d^E)^2}, \qquad (10)$$

only depends on *d*-wave collision properties.

III. RESULTS FOR SODIUM

Sodium collisions are now well understood [4,26–28]. In Ref. [4] an analysis of low intensity spectra led to an accurate determination of the scattering lengths. However, in order to show the additional information available from high

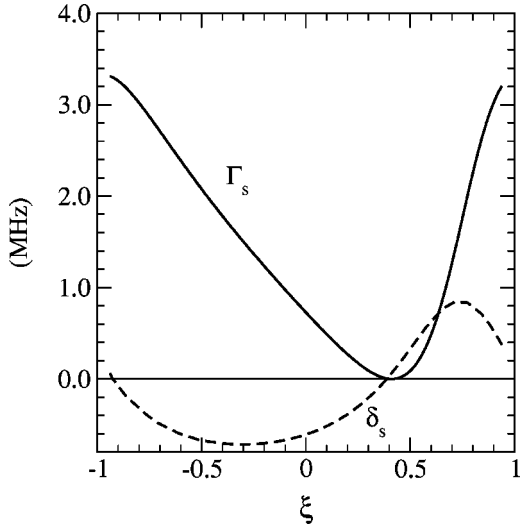

FIG. 2. Excitation rate Γ_s and level shift δ_s for a laser intensity $I=1.0$ W/cm^2 and a collision energy of $E/k_B=500$ μK for Na, as a function of $\xi=(2/\pi)\arctan(a_3/a_{sc})$, with $a_{sc}=90a_0$. A σ^- polarized PA laser excites a pair of doubly spin-polarized atoms colliding in s wave to the $\{0_g^-, v=0, J'=2, M_J'=0\}$ excited state.

intensity spectra relative to the low intensity ones, we will vary the model potential used for the calculations. In particular, we investigate the sensitivity of Γ_l and δ_l to the value of the model scattering length a_3 by adjusting the short-range molecular potential (see Ref. [4]). The precise form of the correction is immaterial at ultracold temperatures.

Figure 2 shows the numerically calculated s wave Γ_s and δ_s for PA to the $\{J'=2\}$ rotational, $\{v=0\}$ vibrational purely long-range 0_g^- state versus the range of variation possible for the model scattering length. The collision energy $E/k_B=500$ μK is a typical collision energy for laser-cooled gases. The figure clearly shows that two potentials with different scattering lengths give rise to the same Γ_s but very different shifts, even with opposite signs. Consequently, in the s-wave limit these two potentials give rise to nearly identical spectra at low intensity but very different spectra at high intensity.

Recall that the zero-energy limit of the bound-continuum contribution to the shift in Eq. (4) is negative. Thereby a positive *zero-energy* s-wave partial shift can only be due to the interaction with an s-wave ground bound state close to threshold, and implies a *positive* s-wave scattering length. However, in Fig. 2 the collision energy E is not zero, and a positive shift is also found for very large and negative scattering lengths, where the bound-bound term is negligible. This is due to the structure, embedded in Γ_s, of the s-wave continuum below the collision energy E. If $|a_3|$ is very large the excitation rate Γ_s drops off rapidly with collision energy (see Ref. [29]) and gives a positive bound-continuum contribution to the shift. Note that shifts and broadening are independent of the atomic density and are absolute quantities which can be measured.

For a closer comparison with current NIST PA experiments that are conducted in a magneto-optical trap (MOT) where the atoms are in their lower hyperfine state, we next fix the model scattering length to the value $a_3=54a_0$, which equals the s-wave scattering length of $\{f_a=f_b=1, f=2\}$, with $\mathbf{f}=\mathbf{f}_a+\mathbf{f}_b$. Although the ground-state scattering wave function for $\{f_a=f_b=1, f=2\}$ collisions is multichannel, the upper hyperfine states are closed about the 0_g^- potential well and do not provide a significant contribution to Γ. In contrast, the level shift δ may have contributions from collision energies where the upper hyperfine states are open and/or from Feshbach resonances in closed channels. Since, in addition, we are simulating the average over all the hyperfine states populated in a MOT by a single effective open channel we can only provide qualitative predictions on the spectra.

Knowledge of a_3 and of the long-range van der Waals coefficient C_6 allows one to predict different threshold properties [30]. In particular, for $a_3=54a_0$ and the value $C_6=1561$ a.u. adopted in this work [31], the model potential supports a d-wave shape resonance at $E_r/k_B\simeq 3.5$ mK. A shape resonance is a long-lived state inside the centrifugal barrier. When the collision energy is close to E_r the atoms can tunnel through the barrier into the PA region and be promoted by the laser to the excited state. It follows from scattering theory and from the Wigner threshold law that the amplitude of the scattering wave function at an arbitrary point in the classically allowed region *inside* the barrier is

$$|\Psi_l^E| \propto \frac{E_r^{l+1/2}}{(E-E_r)+\frac{i}{2}\Gamma_r}, \tag{11}$$

where Γ_r is the collision-energy independent shape-resonance width and in the present situation $l=2$.

Since the partial PA rate Γ_l is at low energy proportional to the square-mod wave function at the Condon point [7], a dramatic increase of Γ_l can be expected at resonance from Eq. (11) when the Condon point is inside the barrier. The lowest vibrational states of the 0_g^- sodium dimer are in the classically forbidden region of the barrier (see Fig. 1), so that Eq. (11) does not strictly apply. A numerical calculation of Γ_d (see Fig. 3) shows, however, a strong resonant feature.

An intuitive description of the system can be given in terms of Fano's configuration interaction (CI) theory [15]. In CI theory our system can be described as a set of two strongly interacting quasi-bound states, the shape resonance and the excited bound state, both interacting with a broad continuum (see Fig. 1). When the (field-dressed) excited state is below the shape-resonance, $(E_{0e}-\hbar\omega)<E_r$, and the two levels are close, the shape-resonance repels the excited state to the red, i.e., closer to threshold and δ is negative. When the field-dressed excited-state is above the shape-resonance, $(E_{0e}-\hbar\omega)>E_r$, and the two levels are close the shape-resonance repels the excited state to the blue, i.e., away from threshold and δ is positive. This argument explains the dispersive shape of the d-wave level shift around E_r, shown in Fig. 3. The s-wave level shift is nearly constant over the same range of collision energies.

Table I shows shifts and stimulated widths calculated per unit laser intensity at a typical collision energy in a MOT, $E/k_B=500$ μK, as a function of the vibrational quantum

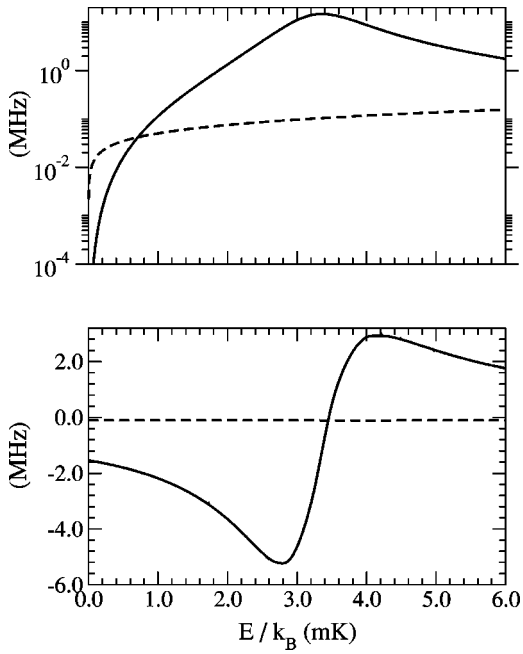

FIG. 3. Energy dependence of laser stimulated rates Γ_l (upper panel) and level shifts δ_l (lower panel) for PA of doubly spin-polarized Na atoms to the $\{0_g^-, v=0, J'=0\}$ excited level and *s*-wave (dashed line) or *d*-wave (full line) collisions. The PA laser is σ^- polarized with an intensity of $I=1.0$ W/cm^2. The model scattering length is $a_3=54a_0$.

number v for $\{J'=2, M_J'=0\}$ rotational quantum numbers and the ground-state partial waves $l=0,2$. Power broadening is dominated by *s* waves while the level shift is mostly due to *d* waves for even v's. The *s*- and *d*-wave collision give in contrast a comparable contribution to the level shift of odd v's. The *g*-wave contribution to both total broadening and shift is negligible. Note the relevance of the bound-bound contribution to the *s*-wave shift for even v's. For odd v's the bound-bound contribution to the level shift is negligible.

This circumstance can be explained by inspecting the ground- and the excited-state wave functions. The ground-state wave function varies relatively slowly over the region where the excited-state wave function is localized. Now, for odd v's the excited-state wave function changes sign an even number of times and the bound-bound overlap integral in Eq. (4) has an equal number of positive and negative contributions that cancel each other to a large extent. For even v's the wave function changes sign an odd number of times and the overlap integral may not be small. The strong *d*-wave partial shift is mostly due to the *d*-wave shape resonance that repels the excited state to the red. Note that this shift arises from collision states that are nearly unpopulated in the trap because of $E/(k_BT)\gg 1$.

We now calculate the actual line shape resulting from thermal averaging. The classical Maxwell-Boltzmann distribution of relative collision velocities is appropriate at typical MOT temperatures. Equation (7) for particles incoming in the state $|l\rangle$ reduces to

$$\mathcal{R}_l=\frac{k_BT}{hQ_T}\int_0^{+\infty}\frac{\gamma\Gamma_l^E e^{-\beta E}}{(E-\Delta-\delta^E)^2+\frac{1}{4}(\gamma+\Gamma^E)^2}\frac{dE}{(k_BT)}, \tag{12}$$

where $Q_T=(2\pi\mu k_BT/h^2)^{3/2}$ is the translational partition function, $\beta=1/(k_BT)$, $\Gamma=\Sigma_l\Gamma_l$ and $\delta=\Sigma_l\delta_l$. It should be emphasized that although the total level shift δ at *fixed* collision energy is the same for all incoming partial waves, due to the dependence of Γ_l on the collision energy, $\Gamma_l \sim E^{l+(1/2)}$, the averaged line shape given by Eq. (12) will have a maximum at a detuning that does depend on *l*, as first pointed out in the low-intensity regime in Ref. [14] and discussed in detail in Ref. [32]. In this low-intensity regime $\Gamma^E\ll\gamma$ and $\delta^E\ll|E-\Delta|$ at each collision energy relevant for the thermal average, and PA line shapes are proportional to the laser intensity. As we increase the intensity Γ and δ may not be negligible at least for some collision energies.

According to a standard definition in bound-bound spectroscopy the saturation intensity is the intensity such that the laser-induced excitation rate equals the spontaneous decay rate. Unlike conventional spectroscopy the saturation intensity, defined for a PA process as $\Gamma^E=\gamma$, depends on collision energy *E*. This energy dependence affects the line shape in a characteristic manner, as we will show for a $\{v=2, J'=4, M_J'=0\}$ excited state. We find negligible *g*- and *h*-wave contributions to the spectral profile of a $J'=4$ level and *d*-waves only must be explicitly considered.

In order to understand the way saturation sets in we plot in Fig. 4 the dimensionless integrand of Eq. (12) as a function of detuning on a suitably spaced energy grid. The lines

TABLE I. Shifts and stimulated rates for Na photoassociation to $\{0_g^-, J'=2, M_J'=0\}$ at collision energy $E/k_B=500$ μK as a function of v. The PA laser is σ^- polarized with intensity $I=1.0$ W/cm^2 and the model scattering length is $a_3=54a_0$. Bound-bound (bb) and continuum bound (bc) contributions to the shift are separately shown. The bound-bound contribution to the shift is negligible for *d* waves. Units are MHz, with powers of ten displayed in brackets.

v	Γ_s	Γ_d	δ_s^{bc}	δ_s^{bb}	δ_d^{bc}
0	3.5[−2]	1.6[−2]	−0.16	5.6[−2]	−1.8
1	6.0[−2]	9.1[−5]	−0.13	9.6[−4]	−0.17
2	7.8[−2]	8.8[−3]	−0.15	2.0[−2]	−0.48
3	0.14	4.1[−4]	−0.19	1.4[−3]	−0.16
4	0.16	8.1[−3]	−0.21	1.0[−2]	−0.48

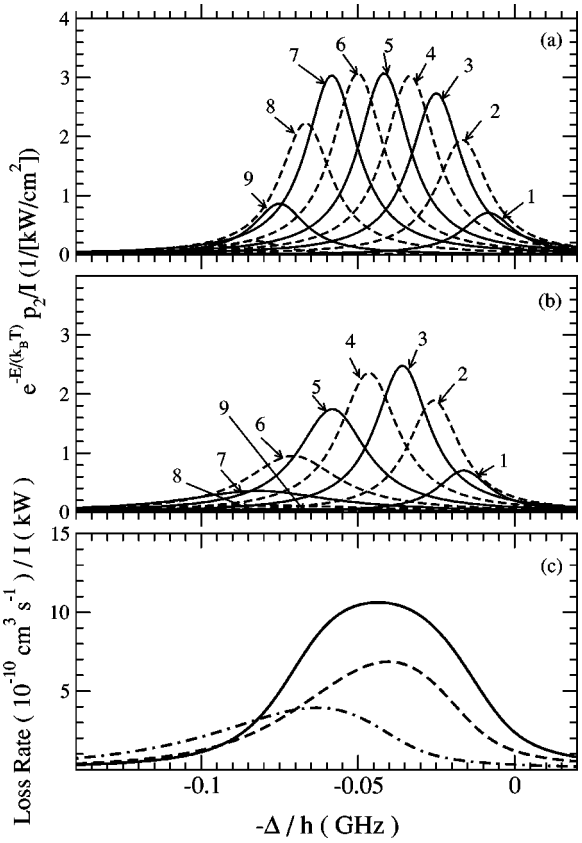

FIG. 4. The integrand of Eq. (12) for Na collisions, $\{0_g^-, v=2, J'=4, M_J'=0\}$ excited state, $T=450$ μK, and the following collision energies E/k_B: 0.4 mK (1), 0.8 mK (2), 1.2 mK (3), 1.6 mK (4), 2.0 mK (5), 2.4 mK (6), 2.8 mK (7), 3.2 mK (8), 3.6 mK (9). The photoassociation laser is σ^- polarized with intensity $I=1.0$ mW/cm^2 (a) and $I=5.0$ W/cm^2 (b). Panel (c) shows the integrated line shape for $I=1.0$ mW/cm^2 (full line), $I=5.0$ W/cm^2 (dashed line), and $I=20.0$ W/cm^2 (dashed-dotted line).

in the top panel of Fig. 4 are unsaturated. Lorentzian curves relative to collision energies around the shape-resonance position are the first to saturate because of the resonance-enhanced excitation rate Γ_d (Fig. 3). At the intensity used in panel (b), $I=5$ W/cm^2, lines 1 and 2 are far from saturation and therefore differ only by a factor proportional to the intensity from the corresponding ones plotted in the upper panel. Saturation shows some effect in line 3 and becomes dramatic for lines 6 to 9, which are strongly suppressed and shifted with respect to the corresponding unsaturated counterparts in panel (a). The line above the shape resonance (line 9) is shifted to the blue with respect to the low intensity ones. It is interesting to notice that although individual lines broaden and shift to the red for most of the collision energies, the integrated line can shift to the blue and its width can decrease, see the dashed line in panel (c) of Fig. 4. This anomalous behavior disappears for higher intensities, where the position of the maximum in the spectral profile is mainly given by the parameter δ in the individual Lorentzians, see the dash-dotted line in panel (c) of Fig. 4.

Also note (Fig. 3) Γ_s is a weaker function of collision energy as compared to Γ_d. Therefore the saturation intensity

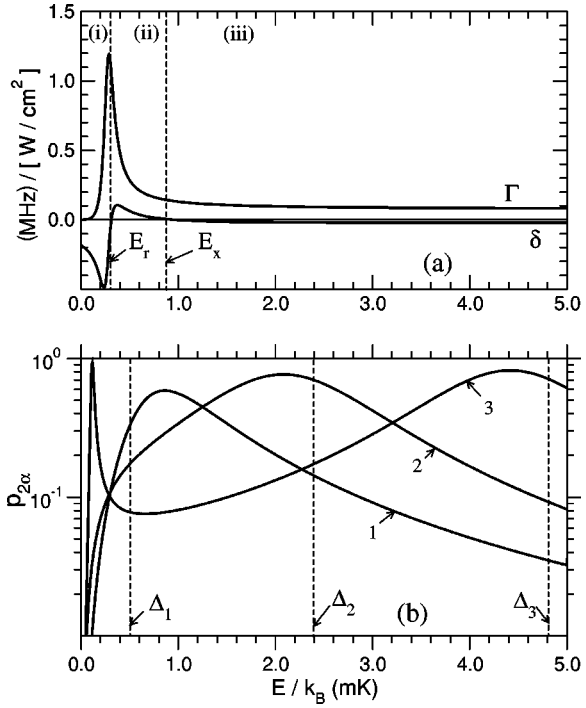

FIG. 5. Panel (a): intensity-normalized shift δ_d and broadening Γ_d as a function of collision energy for PA of doubly spin polarized ^{87}Rb to a $\{0_g^-, v=1, J'=0\}$ excited level. Regions (i), (ii), and (iii) are defined in the text. Panel (b): probability of atom loss for the same transition of panel (a) and a PA laser intensity $I=360$ W/cm^2. The three curves labeled 1,2,3 are for detunings $\Delta_1/h=10$ MHz, $\Delta_2/h=50$ MHz, $\Delta_3/h=100$ MHz, respectively. The vertical lines show the position where the excited-state resonance occurs in the low intensity limit.

of a feature having *s*-wave character depends less on collision energy and the line-shape deformation due to laser power is less pronounced with respect to a feature that has *d*-wave character.

IV. RESULTS FOR RUBIDIUM

Like Na, the scattering properties of Rb atoms are well understood. A triplet scattering length $a_3=100a_0$ and $C_6=4700$ a.u. [31] determines in the ^{87}Rb triplet potential a low-energy *d*-wave shape resonance located at $E_r/k_B \approx 280$ μK [33]. Unlike the case of sodium, the excitation rate and the light shift strongly depend on collision energy within k_BT at typical MOT temperatures (see the upper panel of Fig. 5). Although these resonant features are too narrow to be directly observed in a thermal sample, they have a dramatic influence on the spectrum. In this section we consider a purely *d*-wave transition by the choice of atoms and laser polarization described in Sec. II.

We find it instructive to first discuss the energy dependence of the probability of atom loss $p_{\ell\alpha}$ for different detunings Δ from the excited state (see lower panel of Fig. 5). Please recall that the system can be approximately described as a set of two quasibound states interacting with a broad continuum. We first consider a situation where the resonances are well separated, $(E_{0e}-\hbar\omega-E_r) \gg (\gamma+\Gamma_r)/2$. The

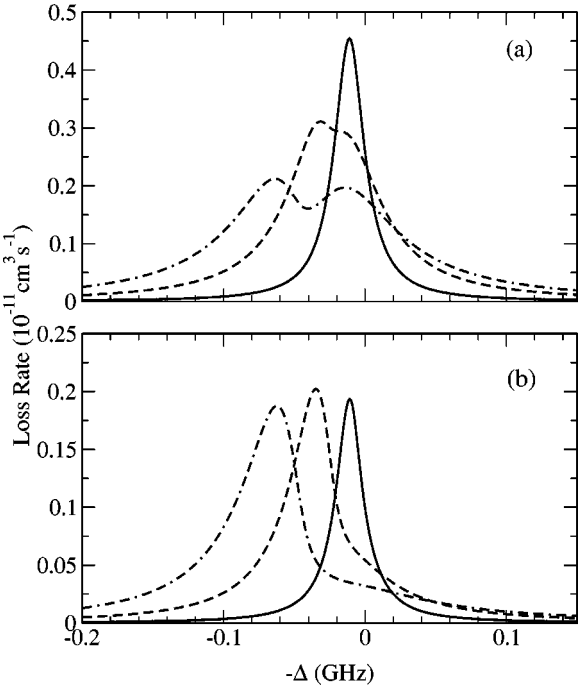

FIG. 6. Saturation in a ^{87}Rb$\{v=1, J'=0,0_g^-\}$ line shape at temperature $T=300$ μK (a), $T=100$ μK, (b), and a laser intensity of $I=20$ W/cm^2 (full line), $I=100$ W/cm^2 (dashed line), and $I=200$ W/cm^2 (dashed-dotted line). The double peak is due to the presence of a low-energy *d*-wave shape resonance in the triplet potential (see text). The peak at small $|\Delta|$ is suppressed at low temperature.

quantity $p_{\ell\alpha}$ shows in this case two peaks (curve 3 in Fig. 6): (i) a low-energy narrow peak related to tunneling of the atoms through the barrier at collision energy $E\sim E_r$, excitation to the excited state and subsequent decay by spontaneous emission, (ii) a high-energy broader peak at collision energy $E\sim(E_{0e}-\hbar\omega)$ related to direct quasiresonant excitation to the excited state and subsequent decay by spontaneous emission. The shape resonance is shifted toward threshold by the interaction with the excited state. Since the two resonances are relatively far detuned, the shift of the excited level is mainly due to the interaction with the continuum and is toward threshold ($\delta<0$, see the upper panel of Fig. 6) as well. Note that the excited level is strongly power broadened.

When the excited state approaches the shape resonance from above the shape resonance further shifts toward threshold and for detunings below $\Delta\simeq|\delta^{E=0}|$ is pushed below threshold and turns into a real bound state (curve 2 in Fig. 6). The shift of the excited level in curve 2 is still determined by the continuum and is negative. However, for smaller detuning (curve 1) the interaction with the shape-resonance dominates and the shift of the excited level is positive.

Let us now evaluate the thermal average of Eq. (12) at a temperature $T\approx E_r/k_B$. In the low-intensity regime the excitation rate Γ in the numerator Eq. (12) behaves approximately like an energy delta function with the center at $E=E_r$ and the integrated line shape is close to a pure Lorentzian with a maximum at $\Delta=E_r$. The line shape is thereby symmetric, in contrast to a situation where the Wigner law holds over all the collision energies relevant for the thermal average [32]. As the intensity I increases, there are two different mechanisms that determine the linewidth. First, Γ increases with I. Second, the level shift δ changes sign across the resonance and provides therefore additional broadening with minor overall shift. Although the latter mechanism gives an apparent broadening, it does not change the area below the spectral curve, as we will show below.

For $I=20$ W/cm^2 (full-line curve in Fig. 6) the line shape is still symmetric. For larger intensities the line deforms in a characteristic manner depending on temperature. We consider a temperature $T=300$ μK and let E_x be the energy at which δ turns from positive to negative (see Fig. 5). It is convenient to separate the three energy components in the integral of Eq. (12): (i) $E\leqslant E_r$ ($\delta\leqslant 0$), (ii) $E_r<E<E_x$ ($\delta>0$), and (iii) $E_x\leqslant E$ ($\delta\leqslant 0$). The relative weights of these components in the thermal average depend both on the Boltzmann factor and on the degree of saturation of the individual Lorentzians falling within each component. Component (i) gives a strongly redshifted contribution to the integrated line shape. Components (ii) and (iii) give a blueshifted or moderately redshifted contribution to the integrated line shape. Note from Fig. 5 that component (ii) is strongly saturated and tends to be suppressed.

For high enough intensity ($I\sim 100$ W/cm^2 for our transition) the different components separate in frequency and the spectral profile develops a double-peak as shown in the upper panel of Fig. 6. Since the peak located at larger $|\Delta|$ corresponds to relatively small energies in the thermal average its position is weakly temperature dependent. The peak located at small $|\Delta|$ is mostly due to the high-energy component (iii). At large collision energy Γ^E and δ^E are relatively small and the contribution of (iii) to the total line shape tends to be proportional to the laser intensity. In particular the peak position is weakly intensity dependent. The position of the dip between the peaks is approximately linear with the laser intensity. The peak ratio is strongly dependent on temperature, the small-detuning (high-energy) peak being suppressed at low T, as shown in the lower panel of Fig. 6. Note, however, the tail at $(-\Delta)>0$ which corresponds to collision energies falling within component (ii).

The resonance position can be extracted from saturated line shapes by analyzing the line shape in terms of the area enclosed below the spectral curve. This area is

$$\mathcal{A}(I,T)=\int (d\Delta)\mathcal{R}(\Delta,I,T)$$

$$=2\pi\frac{k_BT}{hQ_T}\int_0^\infty dE e^{-\beta E}\frac{\gamma\Gamma_d^E}{(\gamma+\Gamma_d^E)},$$

where the integral over Δ has been extended to all the real axis. As anticipated the area is independent of the level shift. If the coefficient of proportionality relating the theoretical loss rate $\mathcal{R}$ to the measured one was accurately known, the area $\mathcal{A}$ could provide information on the integral of Γ_d, i.e., on the strength of the resonance, already in the low-intensity regime. For high intensities we can in contrast get rid of this proportionality factor by comparing $\mathcal{A}$ in the saturation re-

gime with a reference low intensity value. To this aim we define an intensity normalized integrated line shape x, normalized to the zero intensity value

$$x(I,T)=\frac{\mathcal{A}(I,T)}{I}\lim_{I\to 0}\frac{I}{\mathcal{A}(I,T)}.$$

We show in Fig. 7 three different curves representing the calculated quantity x as a function of the laser intensity for different resonance positions. Note the sensitivity of these curves to the resonance position over a range of intensities easily accessible experimentally. We also find these integrated line shapes to very good approximation independent of temperature at typical MOT temperatures.

V. SUMMARY

We have discussed a systematic approach to treat binary collisions in the presence of an intense laser field that fully includes the multichannel hyperfine aspect of the problem and coupling of different partial waves. Saturation manifests itself in characteristic line shapes when a thermal gas is photoassociated by an intense field. The presence of a shape resonance at thermal energy can lead to the appearance of a double peak in the spectrum.

We have shown how analysis of these intensity spectra can significantly help constrain collisional ground-state models or provide a cross-check of the potential when this is already known. In particular, few measurements of the level shift can in some cases give strong information on, or even determine the sign, of the scattering length.

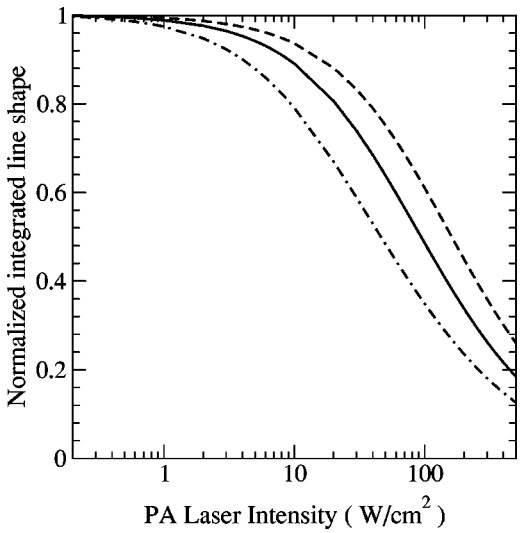

FIG. 7. Intensity normalized integrated line shape for PA of doubly spin-polarized ^{87}Rb, d-wave collisions, $\{0_g^-, v=1, J'=0\}$ excited state, and different positions of a d-wave shape resonance: $E_r/k_B=280\ \mu$K ($a_3=100a_0$, full line), $E_r/k_B=430\ \mu$K ($a_3=114a_0$, dashed line), $E_r/k_B=180\ \mu$K ($a_3=91a_0$, dashed-dotted line). Temperature is $T=450\ \mu$K and the PA laser is σ_z polarized.

ACKNOWLEDGMENTS

We acknowledge F. H. Mies for several useful discussions, and K. M. Jones and F. K. Fatemi for providing us with high intensity PA experimental data for sodium. A.S. thanks NIST, Gaithersburg, for kind hospitality and partial support.

[1] H.R. Thorsheim, J. Weiner, and P.S. Julienne, Phys. Rev. Lett. **58**, 2420 (1987).
[2] J.D. Miller, R.A. Cline, and D.J. Heinzen, Phys. Rev. Lett. **71**, 2204 (1993).
[3] E.R.I. Abraham, N.W.M. Ritchie, W.I. McAlexander, and R.G. Hulet, J. Chem. Phys. **103**, 7773 (1995).
[4] E. Tiesinga, C.J. Williams, P.S. Julienne, K.M. Jones, P.D. Lett, and W.D. Phillips, J. Res. Natl. Inst. Stand. Technol. **101**, 505 (1996).
[5] C.J. Williams, E. Tiesinga, P.S. Julienne, H. Wang, W.C. Stwalley, and P.L. Gould, Phys. Rev. A **60**, 4427 (1999).
[6] J.P. Burke, Jr., C.H. Greene, J.L. Bohn, H. Wang, P.L. Gould, and W.C. Stwalley, Phys. Rev. A **60**, 4417 (1999).
[7] P.S. Julienne, J. Res. Natl. Inst. Stand. Technol. **101**, 487 (1996).
[8] K.M. Jones, S. Maleki, L.P. Ratliff, and P.D. Lett, J. Phys. B **30**, 289 (1997).
[9] H.M.J.M. Boesten, C.C. Tsai, D.J. Heinzen, A.J. Moonen, and B.J. Verhaar, J. Phys. B **32**, 287 (1999).
[10] J.L. Bohn and P.S. Julienne, Phys. Rev. A **60**, 414 (1999).
[11] J.M. Gerton, B.J. Frew, and R.G. Hulet, Phys. Rev. A **64**, 053410 (2001).
[12] C. McKenzie, J. Hecker Denschlag, H. Häffner, A. Browaeys, Luís E.E. de Araujo, F.K. Fatemi, K.M. Jones, J.E. Simsarian, D. Cho, A. Simoni, E. Tiesinga, P.S. Julienne, K. Helmerson, P.D. Lett, S.L. Rolston, and W.D. Phillips, Phys. Rev. Lett. **88**, 120403 (2001).
[13] P.O. Fedichev, Yu. Kagan, G.V. Shlyapnikov, and J.T.M. Walraven, Phys. Rev. Lett. **77**, 2913 (1996).
[14] R. Napolitano, J. Weiner, C.J. Williams, and P.S. Julienne, Phys. Rev. Lett. **73**, 1352 (1994).
[15] U. Fano, Phys. Rev. **124**, 1866 (1961).
[16] C. Cohen-Tannoudji, J. Dupont-Roc, and G. Grymberg, *Atom-Photon Interactions: Basic Processes and Applications* (Wiley, New York, 1992).
[17] F.H. Mies, in *Theoretical Chemistry: Advances and Perspectives*, edited by D. Henderson (Academic, New York, 1981), pp. 127–198.
[18] H.M.J.M. Boesten, B.J. Verhaar, and E. Tiesinga, Phys. Rev. A **48**, 1428 (1993).
[19] P.S. Julienne, K.-A. Suominen, and Y.B. Band, Phys. Rev. A **49**, 3890 (1994).
[20] P.S. Julienne and F.H. Mies, J. Opt. Soc. Am. B **6**, 2257 (1989).
[21] R.W. Montalvão and R.J. Napolitano, Phys. Rev. A **64**, 011403 (2001).
[22] J.R. Taylor, *Scattering Theory* (Wiley, New York, 1972).
[23] H. Feshbach, *Theoretical Nuclear Physics* (Wiley, New York, 1992).

[24] C.J. Williams, E. Tiesinga, and P.S. Julienne, Phys. Rev. A **53**, R1939 (1996).
[25] E.P. Wigner, Phys. Rev. **73**, 1002 (1948).
[26] F.A. van Abeelen and B.J. Verhaar, Phys. Rev. A **59**, 578 (1999).
[27] A. Crubellier, O. Dulieu, F. Masnou-Seeuws, M. Elbs, H. Knöckel, and E. Tiemann, Eur. Phys. J. D **6**, 211 (1999).
[28] C. Samuelis, E. Tiesinga, T. Laue, M. Elbs, H. Knöckel, and E. Tiemann, Phys. Rev. A **63**, 012710 (2001).
[29] M. Machholm, P.S. Julienne, and K.-A. Suominen, Phys. Rev. A **65**, 023401 (2002).
[30] B. Gao, Phys. Rev. A **58**, 1728 (1998).
[31] A. Derevianko, J.F. Babb, and A. Dalgarno, Phys. Rev. A **63**, 052704 (2001).
[32] K.M. Jones, P.D. Lett, E. Tiesinga, and P.S. Julienne, Phys. Rev. A **61**, 012501 (2000).
[33] P.J. Leo (private communication).